https://doi.org/10.1016/j.ijhydene.2018.09.023

Enhanced capacitive performance of nickel oxide on porous $La_{0.7}Sr_{0.3}CoO_{3-\delta}$ ceramic substrate for electrochemical capacitors

Peipei Liu[a,b], Zhijun Liu[a], Peng Wu[a], Xing Ou[a], Yapeng Zhang[a], Weizi Cai[a,b], Fangyong Yu[a,c], Meng Ni[b,*], Shuang Cheng[a], Meilin Liu[a,d], Jiang Liu[a,*]

[a] *Guangzhou Key Laboratory for Surface Chemistry of Energy Materials, New Energy Research Institute, School of Environment and Energy, South China University of Technology, Guangzhou 510006, China.*

[b] *Building Energy Research Group, Department of Building and Real Estate, The Hong Kong Polytechnic University, Hung Hom, Kowloon, Hong Kong, China*.

[c] *School of Chemical Engineering, Shandong University of Technology, Zibo 255049, China.*

[d] *School of Materials Science and Engineering, Georgia Institute of Technology, 771Ferst Drive, Atlanta, GA 30332-0245, USA.*

*Corresponding author:

E-mail: meng.ni@polyu.edu.hk, jiangliu@scut.edu.cn

Abstract

Nickel oxide (NiO) nanoparticles loaded on porous strontium-substituted lanthanum cobaltite ($La_{0.7}Sr_{0.3}CoO_{3-\delta}$, LSC) ceramic substrate is fabricated as a novel binder-free electrode (NiO/LSC) for electrochemical capacitors. The LSC substrate is synthesized through a simple solid-state method. NiO nanoparticles are loaded onto the porous LSC substrate by infiltrating a nickel nitrate ($Ni(NO_3)_2$) solution into the pores, followed by calcination. The composite electrode NiO/LSC with a high mass loading of NiO (~10 mg cm^{-2}) exhibits an appreciable areal capacitance of 10.6 F cm^{-2}, a specific capacitance of 1064.1 F g^{-1} and remarkable cycling stability (80.1% retention after 3000 cycles at 20 mA cm^{-2}). Moreover, an asymmetric electrochemical capacitor, with

NiO/LSC as the positive electrode and carbon cloth as the negative electrode, confirms the excellent capacitive properties, with high energy density of 9.27 mWh cm^{-3} under a wide potential of 1.65 V. This work indicates the promising application of NiO/LSC as an advanced electrode for electrochemical capacitors.

Keywords: Electrochemical capacitors； Electrode; NiO; $La_{0.7}Sr_{0.3}CoO_{3-\delta}$ substrate

1. Introduction

Effective energy storage devices play an important role in application of renewable and sustainable resources, such as solar and wind energy. Electrochemical capacitors, which also called supercapacitors or ultracapacitors, have become one of compelling candidates due to their high power density, long cycling life and rapid charge/discharge rate [1,2]. In the past decades, they have been widely used as auxiliary or standalone power supply for portable devices, electric buses and smart grids etc.. Generally, according to energy storage mechanism, electrochemical capacitors can be classified into two types: electrical double layer capacitors (EDLCs) and pseudocapacitors [3]. Compared to the EDLCs, which store energy only through adsorption/desorption of ions at the surface of electrode materials, pseudocapacitors can make use of rapid reversible surface or near surface redox reactions to offer 3~4 times higher capacitance [4,5]. In addition, as one of vital and indispensable components, various kinds of electrode materials have been extensively studied to enhance capacitive performance of electrochemical capacitors.

Transition metal oxides, such as manganese oxide [6], cobalt oxide [7], nickel oxide [8] and iron oxide [9], are typical pseudocapacitive electrode materials. Among them, NiO has attracted increasing attention in recent years, owing to its multiple oxidation states (Ni^{2+}/Ni^{3+}) [10], low cost (compared to RuO_2-based electrodes) [11] and promising theoretical capacitance (~2584 F g^{-1}, within a potential window of 0.5

V) [12]. In general, NiO-based working electrodes for electrochemical capacitors are prepared through mixing with PTFE or PVDF (as a binder) and carbon black (as a conductive agent), and then coating or pressing onto a current collector. However, this method gives rise to limited active sites for the redox reaction and high electrical contact resistance between the electrode material and current collector, resulting in relatively poor capacitive performance. For instance, Ren et al. [13] reported NiO-based electrode with a low capacitance of 181 F g^{-1} at the current density of 20 mA cm^{-2} and Du et al. [14] reported Ni@NiO-based electrode with a poor rate capability (the retention is only 19% from 1 to 10 A g^{-1}), which both were prepared by the steps as above mentioned. Therefore, NiO electrode materials directly grown or loaded on conductive substrates (i.e., current collectors) has become an alternative method [15,16].

Recently, Wu et al. [17] prepared NiO nanoflake arrays directly grown on nickel foam and obtained the largest specific capacitance of 2013.7 F g^{-1} at 1 A g^{-1}. However, the mass loading of NiO on the nickel foam substrate is only 1.15 mg cm^{-2} under a potential window from 0.0 to 0.5 V (vs. SCE), which is far less than the commercial value of 10 mg cm^{-2} to obtain realistic capacitance, as pointed by Yu [18] and Gogotsi [19]. Therefore, the search for an appropriate substrate that can directly load NiO with a commercial level mass loading is urgent and significant. The perovskite oxide $LaCoO_3$ is an attractive ceramic material that has been widely used as a cathode for fuel cells [20,21], a catalyst for the combustion of volatile organic compounds [22,23] and a thermoelectric material [24,25]. In addition, the electrical conductivity of $LaCoO_3$ can be improved by Sr^{2+} partially substituting for La^{3+} [26], because the Co-O-Co bond angle becomes closer to 180 °, which is caused by the larger overlap and the stronger interactions between the Co(3d)-O(2p) orbitals, thereby increasing the carrier mobility [27,28]. Moreover, Petrov et al. have demonstrated the high conductivity of the

$La_{0.7}Sr_{0.3}CoO_{3-\delta}$ at low temperature (333 K) [29]. Therefore, it is reasonable to believe that a novel substrate loaded with NiO may be used as an electrode for high performance electrochemical capacitors.

Herein, we report on the direct loading of NiO nanoparticles onto a porous $La_{0.7}Sr_{0.3}CoO_{3-\delta}$ ceramic substrate (NiO/LSC) through a solid-state method and an infiltration process. To the best of our knowledge, this is the first study on the capacitive performance of NiO/LSC as an electrode for electrochemical capacitors. The porous LSC ceramic substrate not only improves the conductivity of the prepared electrode, but also enables a high mass loading of NiO (the optimal mass loading reaches up to ~10.0 mg cm^{-2}). As expected, both the single electrode NiO/LSC and the designed asymmetric electrochemical capacitor (NiO/LSC as the positive electrode and carbon cloth (CC) as the negative electrode) exhibit large areal and specific capacitance, high energy density and excellent stability. To confirm the optimal mass loading, we examine the capacitive properties of various mass loadings of NiO on LSC. In addition, the electrochemical performance of NiO with a mass loading of ~10 mg cm^{-2} on a traditional Ni foam substrate is studied for comparison.

2. Experimental section

Lanthanum oxide (La_2O_3), ethanol, polyvinyl butyral (PVB), starch and nickel nitrate hexahydrate ($Ni(NO_3)_2.6H_2O$) were purchased from Sinopharm Chemical Reagent Co., Ltd. Strontium carbonate ($SrCO_3$) and cobalt oxide (Co_3O_4) were obtained from Guangzhou Chemical Reagent Co., Ltd. and Aladdin Chemical Co., Ltd., respectively. All these reagents were of analytical grade.

Ni foam (1.00 × 1.00 × 0.05 cm) was bought from Kunshan Jiayisheng Electronics Co., Ltd. It was rinsed with deionized water and ethanol after being washed in 0.1 M hydrochloric (HCl) and acetone. Then, Ni foam of high purity was obtained after drying

at 80 °C in a vacuum drying oven. CC wafer (diameter of 1.00 cm and thickness of 0.02 cm) was purchased from Shanghai Hesen electric Co., Ltd. and was pre-calcined in air at 400 °C for 2 h.

2.1. Synthesis of porous LSC substrate

LSC pellets were prepared through a solid-state method. Firstly, La_2O_3 was pre-calcined at 1000 °C for 2 h to remove water. Secondly, according to the stoichiometric ratio in $La_{0.7}Sr_{0.3}CoO_{3-\delta}$, the desired amount of La_2O_3, $SrCO_3$ and Co_3O_4 were mixed through ball milling for 8 h. After that, the mixture was mixed with 15 wt.% starch (as a pore former) in ethanol solvent by ball milling for 2 h, and then mixed with 3 wt.% PVB (as a binder) by grinding in a mortar for 30 min. Then, the mixture was dried and pressed into pellets under a pressure of ~300 MPa using a stainless steel mold (1.3 cm in diameter). Eventually, the pellets were fired at 1100 °C for 12 h in air to obtain LSC substrates. The average weight, diameter and thickness of the pellets were 0.15 g, 1.16 cm and 0.05 cm, respectively. The porosity of the porous LSC substrate was ~38.9%, based on Archimedes' method [30].

2.2. Preparation of NiO/LSC electrode

NiO nanoparticles were directly loaded on porous LSC by an infiltration process, followed by calcination. The prepared LSC pellet was submerged into a 0.5 M $Ni(NO_3)_2$ solution for 20 s, and then dried in a vacuum drying oven at 140 °C for 20 min. This process was repeated several times to obtain a required mass loading of NiO. Then, the samples were calcined at 500 °C in an argon atmosphere for 1 h to obtain the NiO/LSC electrode. To search for the optimal mass loading, three samples with NiO loadings of 5.1, 10.0 and 15.2 mg cm^{-2} were prepared and denoted as 5NiO/LSC, 10NiO/LSC and 15NiO/LSC, respectively. For comparison, NiO (with a mass loading of ~10 mg cm^{-2})

deposited on a Ni foam substrate (denoted as 10NiO/Ni-F) was fabricated using the same method.

2.2.Characterization

X-ray diffraction (XRD, Bruker D8 Advance diffractometer with Cu Kα (λ=0.15418 nm) radiation, field emission scanning electron microscope (FESEM, Merlin, 5.0 kV), and transmission electron microscopy (TEM, JEOL JEM-2100) were employed to identify the crystallinity, morphology and structure of the prepared samples, respectively. X-ray photo spectroscopy (XPS, Escalab 250, Al Kα) was used to analyze the elemental compositions and the chemical states of the products.

2.3.Electrochemical measurements of NiO/LSC electrode

A CHI600E (Shanghai Chenhua) electrochemical station was applied for electrochemical measurements of the single prepared NiO/LSC electrode (working electrode), using a three-electrode system in a 6.0 M KOH solution. Hg/HgO and Pt mesh (1 cm^2) were used as reference and counter electrodes, respectively. Cyclic voltammetry (CV) tests were studied at different scan rates between the potential of −0.3 and 0.6 V. Galvanostatic charge-discharge curves were recorded from –0.3 to 0.5 V. Electrochemical impedance spectra (EIS) were measured in the 0.01 Hz to 10 MHz frequency range.

2.4.Fabrication and test of an asymmetric electrochemical capacitor

An asymmetrical electrochemical capacitor (NiO/LSC//CC) was designed using cellulose paper as the separator in a 6 M KOH electrolyte solution. The effective area and total thickness of the fabricated device are 1.05 cm^2 and 0.07 cm, respectively. Its electrochemical performances were recorded under a voltage of 1.65 V, using the same electrochemical work station (CHI600E). The capacitance (C), energy density (E) and power density (P) of the single electrode and assembled device were calculated

according to the following equations [31]:

$$C = \frac{it}{V} \qquad (1)$$

$$E = \frac{1}{2}CV^2 \qquad (2)$$

$$P = \frac{E}{t} \qquad (3)$$

where C (F cm^{-2} or F g^{-1}), i (mA cm^{-2}) and V (V) are the capacitance, the current density, and the potential window, respectively. t (s) is the time during discharge process. E (mWh cm^{-3} or Wh kg^{-1}) and P (mW cm^{-3} or W kg^{-1}) are the energy density and power density, respectively.

3. Results and discussion

Several factors may affect capacitive performance of porous LSC ceramic substrate supported NiO nanoparticles as the electrode for electrochemical capacitors, including features of the prepared materials like crystal structure, microstructure, valence situation and the interaction between NiO and LSC. Detailed investigations on these correlations are carried out, as in the following.

3.1.Crystalline phase and composition analysis

Fig. 1a shows the phase information for LSC and NiO/LSC. The pattern of the prepared LSC is in good accordance with the standard pattern of the rhombohedral $La_{0.7}Sr_{0.3}CoO_{3-\delta}$ phase (JCPDS no. 89-4462). For the NiO/LSC sample, besides the peaks of LSC, there are three other diffraction peaks at 2θ degrees of 37.2°, 43.3°, and 62.9°, which can be assigned to the (111), (200) and (220) crystal planes of the cubic NiO phase (JCPDS no. 71-1179), respectively. It is noted that the strongest peak of LSC shift slightly after the loading of NiO, as displayed in Fig. 1b, implying the interaction and strong adhesion between the porous substrate and NiO active material.

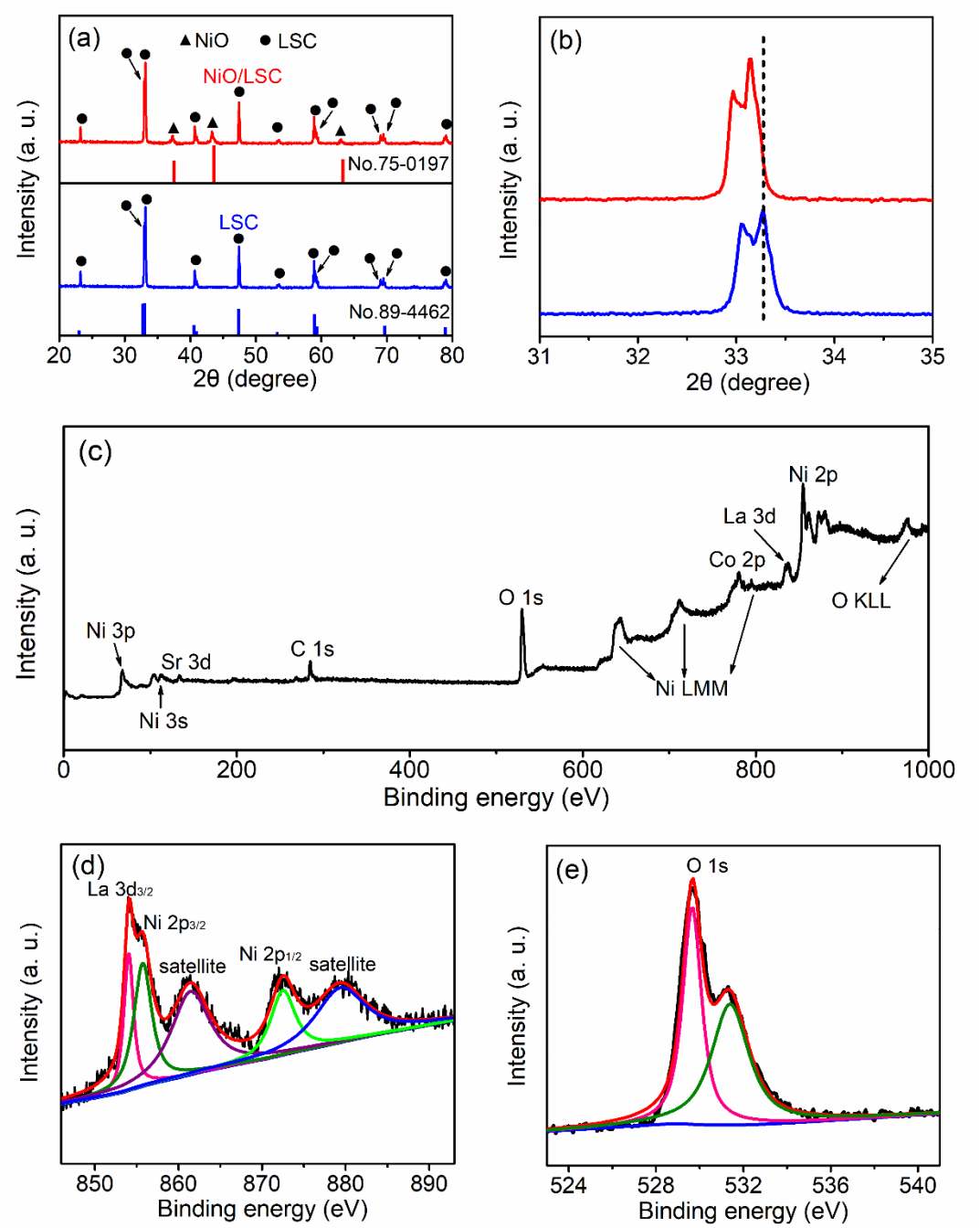

Fig. 1. (a) XRD patterns and (b) the most peak intensities of LSC and NiO/LSC. (c) XPS survey spectrum of NiO/LSC. (d) Ni 2p core level spectrum. (e) O 1s core level spectrum.

The wide survey XPS spectrum proves the presence of La, Sr, Co, O and Ni in NiO/LSC, as exhibited in Fig. 1c. Fig.1d shows the highly resolved narrow scan of Ni 2p core level spectrum. The main peak at 854.0 eV for Ni $2P_{3/2}$ and the peak at 872.5 eV for Ni $2P_{1/2}$ imply the presence of Ni^{2+} in NiO [11,32]. In addition, the shakeup

satellite peaks located at 861.7 and 879.4 eV can be attributed to the fingerprint of the electronic structures of NiO [33]. Notably, a weaker peak at 855.7 eV can be identified, which is resulted from the nickel hydroxides or nickel oxyhydroxides [34,35]. For the O 1s, there are two deconvoluted peaks, as displayed in Fig. 1e. The peak situated at 529.5 eV is a typical state of O^{2-} specie in metal oxide, while the peak at 531.4 eV is ascribed to absorbed H_2O on the surface of the NiO/LSC [36,37].

3.2.Microstructural characterizations

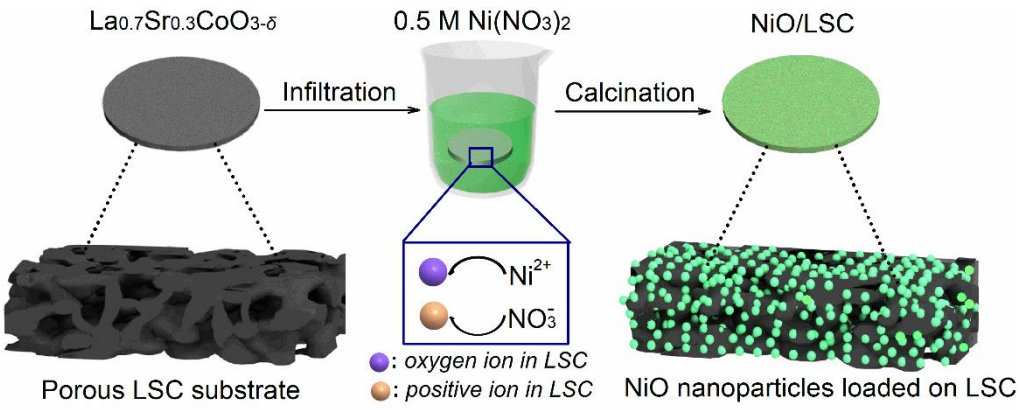

Fig. 2. Schematic illustration of the NiO nanoparticles loaded on porous LSC.

An illustration of the prepared NiO/LSC is shown in Fig. 2. NiO nanoparticles loaded on the porous LSC ceramic substrate can be easily obtained through infiltration and calcination steps. Fig. 3 shows the cross-sectional SEM and HRTEM images of LSC and NiO/LSC. The LSC substrate is porous with a pore size of the order of ~ 1 μm (Figs. 3a and b). Fig. 3c shows the HRTEM image of the LSC. The inter-planar spacing of 0.269 nm is attributed to the (104) facet of rhombohedral LSC. Fig. 3d and e display the SEM images of the porous LSC substrate loaded with NiO. It can be seen that NiO nanoparticles, with a size of ~10 nm, are uniformly distributed on the inner surface of the porous LSC ceramic substrate. The formation of this favorable structure can be attributed to the electrostatic force [11]. During the infiltration process, Ni^{2+} is selectively combined with the O^{2-} of LSC, while NO_3^- is attracted by the positive ion

of the ceramic substrate, ensuring NiO nanoparticles bond tightly with porous LSC after calcination. The HRTEM image of the NiO nanoparticles is shown in Fig. 3f. The inter-planar spacing of 0.209 nm is attributed to (200) facet of cubic NiO.

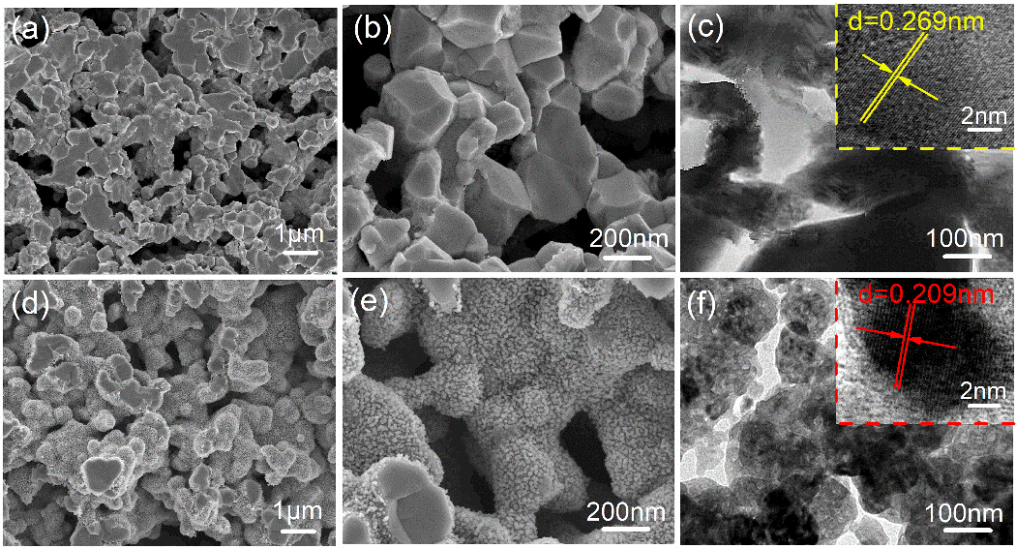

Fig. 3. Cross-sectional SEM and HRTEM images of (a-c) LSC and (d-f) NiO/LSC.

3.3.Electrochemical performance of NiO/LSC

Fig. 4(a) shows comparison of the capacitive behaviors of LSC, 5NiO/LSC, 10NiO/LSC and 15NiO/LSC at a scan rate of 10 mV s^{-1}. It can be seen that the CV curve of the bare LSC present much smaller quasi-rectangular. Conversely, for NiO/LSC electrodes, the CV curves have well-defined cathodic and anodic peaks, which are caused by the redox reaction (eq. 4) [38]:

$$NiO + OH^- \Leftrightarrow NiOOH + e^- \qquad (4)$$

Clearly, the area enclosed by the curve of 10NiO/LSC is the largest, suggesting that its capacitance is higher than those of 5NiO/LSC and 15NiO/LSC. Meanwhile, the discharge time of 10NiO/LSC is longer than those of the three other electrodes, as can be observed from the galvanostatic charge-discharge curves at 10 mA cm^{-2} in Fig. 4b. Besides, the capacitive contribution of LSC to the composite NiO/LSC is negligible (the electrochemical properties of the bare LSC can be seen in Fig. S1). Of these

samples, the 10NiO/LSC shows the best capacitive performance, indicating that the optimal mass loading of NiO nanoparticles on the porous LSC ceramic substrate is ~10 mg cm^{-2}.

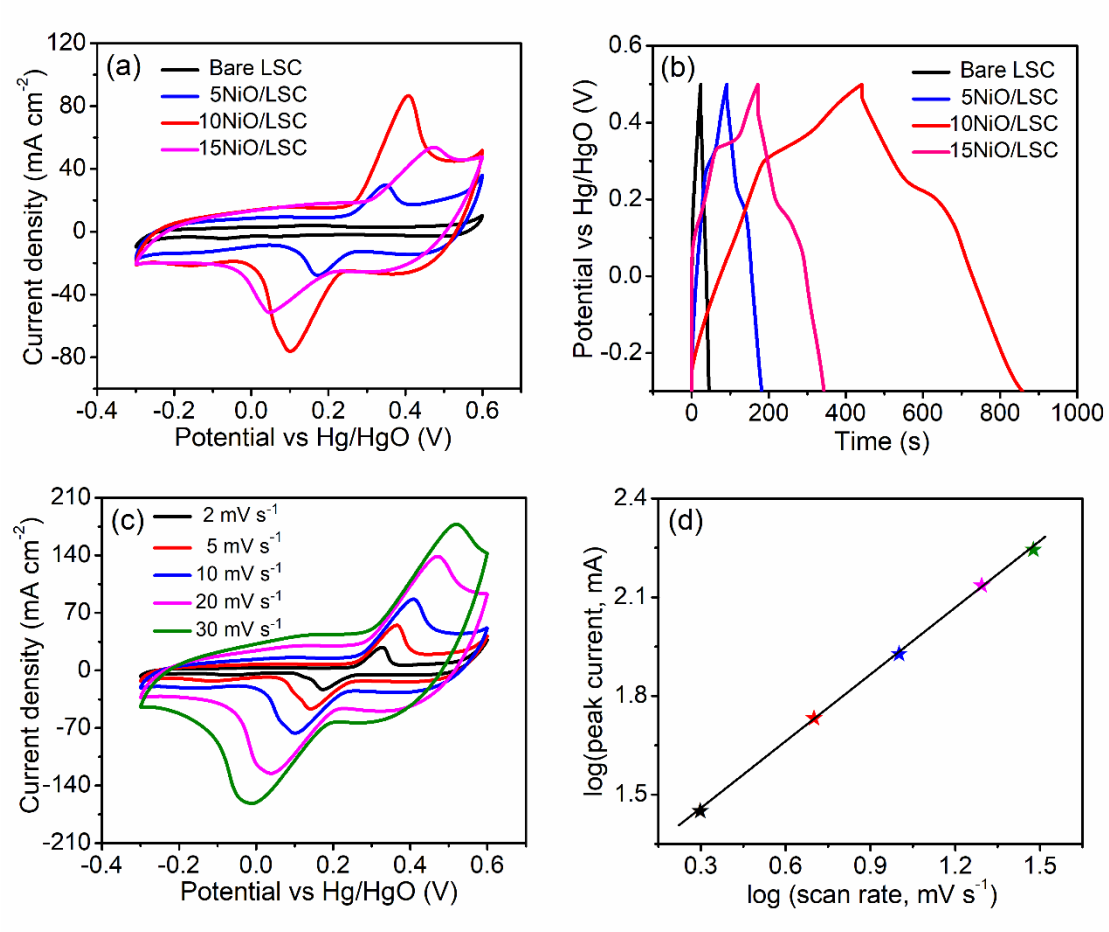

Fig. 4. (a) CV curves at 10 mV s^{-1} and (b) galvanostatic charge-discharge profiles at 10 mA cm^{-2} for bare LSC, 5NiO/LSC, 10NiO/LSC and 15NiO/LSC. (c) CV curves at various scan rates and (d) relationship between peak current densities and scan rates for 10NiO/LSC.

As mentioned, for the NiO/LSC electrode, the active material contributing to the major capacitance is NiO, which performs the redox reaction (eq. 4). The functions of the porous LSC ceramic substrate are supporting the NiO nanoparticles and conducting electricity. The capacitance variation with NiO mass can be explained according to the

micromorphology, as shown in Fig. S2. For both of 5NiO/LSC and 10NiO/LSC, the NiO nanoparticles distribute evenly on the inner surface of the pores. The active NiO nanoparticles of 10NiO/LSC are more than those of 5NiO/LSC, resulting in the capacitance of the former being higher than the latter. However, the NiO nanoparticles aggregate together when the mass loading increases to 15 mg cm^{-2} and the pore channel of the LSC substrate is blocked, hindering the transport of ions and electrons, and leading to poor capacitive behavior.

Fig. 4c shows the typical CV curves of 10NiO/LSC at scan rates from 2 to 30 mV s^{-1}. A pair of obvious redox peaks can be observed with a 6 M KOH solution as the electrolyte, confirming good rates of the ionic and electronic transport in the electrochemical process between potentials of −0.3 and 0.6 V. Additionally, the mechanism of the charge storage can be analyzed according to eq. 5 [39]:

$$i = av^b \qquad (5)$$

where i and v represent the measured peak current density and scan rate, respectively, while a and b are both adjustable parameters. The b value can be evaluated by the slope of log$i$ versus log$v$, a value of 0.5 means ideal diffusion-controlled process and a value close to 1 indicates a capacitive nature. Fig. 4d displays the log(v)-log(i) plot for the prepared 10NiO/LSC electrode. The calculated b value is ~0.7, suggesting a hybrid electrochemical behavior incorporating both capacitive storage and a diffusion-controlled process [40].

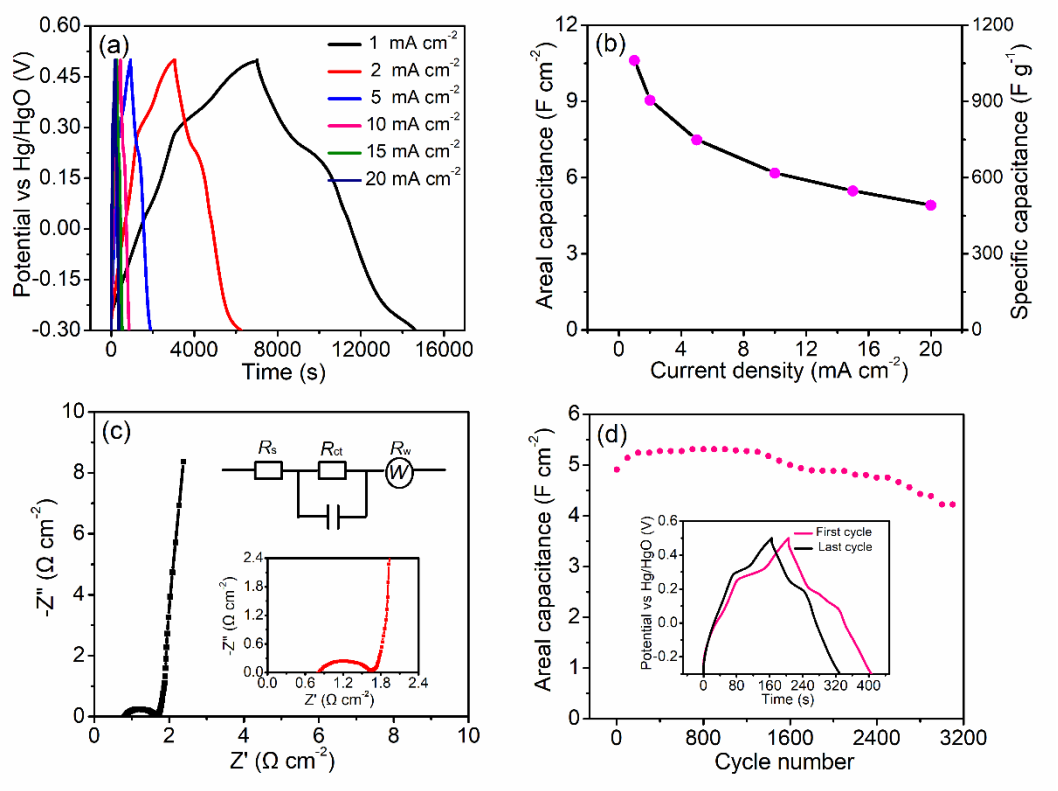

Fig. 5. (a) Galvanostatic charge-discharge curves, (b) areal and specific capacitances at different current densities, (c) EIS spectra (the insets are corresponding equivalent circuit and the enlarged high-frequency region, respectively) and (d) cycle performance at 20 mA cm^{-2} (the inset is galvanostatic charge-discharge profiles before and after 3000 cycles) of 10NiO/LSC.

To evaluate the electrochemical properties of 10NiO/LSC, galvanostatic charge-discharge curves are measured in a potential range from −0.3 to 0.5 V at various current densities, as exhibited in Fig. 5a. These are obvious non-linear curves during charge and discharge process, which are in agreement with the redox peaks of the above CV curves (in Fig. 4c). The calculated areal and specific capacitance according to discharge profiles are presented in Fig. 5b. The values are as high as 10.6 F cm^{-2} and 1064.1 F g^{-1} at 1 mA cm^{-2}, respectively. Even the current density increases 20 times (i.e. 20 mA cm^{-2}), the areal and specific capacitance are still up to 4.9 F cm^{-2} and 492.7 F g^{-1},

respectively, suggesting good rate capability of the prepared 10NiO/LSC electrode.

Fig. 5c displays the Nyquist plots of 10NiO/LSC. The EIS spectra can be divided into three parts, as shown in the enlarged region (the inset of Fig. 5c). The intercept on the real axis and the diameter of the semicircle in the high frequency indicate bulk resistance (R_s) and charge transfer impedance (R_{ct}), respectively [16,41], as shown in the inset of Fig. 5c (the corresponding equivalent circuit). The estimated values of R_s and R_{ct} are as small as 0.81 and 0.80 Ω cm^2, respectively, because the well-distributed NiO nanoparticles are in tight contact with the highly conductive LSC substrate [42]. Meanwhile, the vertical straight line in the low frequency region represents the Warburg resistance (R_w), implying a fast ion diffusion rate in the porous structure of 10NiO/LSC. The cycling stability was also conducted to estimate the capacitive performance of 10NiO/LSC, as exhibited in Fig. 5d. It reveals that the areal capacitance remains 80.1% after 3000 cycles at 20 mA cm^{-2}.

The electrochemical properties of NiO loaded on the porous ceramic LSC substrate as an electrode are superior to previously reported transition metal oxides on traditional substrates, as listed in Table 1. The excellent properties can be ascribed to the following facts: (1) the porous structure, stable characteristic and high conductivity of the LSC substrate, ensuring effective utilization of the active material; (2) NiO with a high mass loading (10 mg cm^{-2}) on the porous LSC substrate, resulting in outstanding areal capacitance; (3) strong adhesion and suitable compatibility between NiO nanoparticles and the porous LSC ceramic substrate, which can maintain stability during the continuous galvanostatic charge-discharge process.

Table 1. Electrochemical performance of 10NiO/LSC compared with previously reported electrodes.

Sample/ substrate	Mass loading (mg cm^{-2})	Areal capacitance (F cm^{-2})	Specific capacitance (F g^{-1})	Cycling stability	Ref.
NiO/Cu foil	0.327	0.29 (0.36mA cm^{-2})	895.05	87.9% (3000 cycles)	[16]
NiO/Ni foam	~10	3.26 (20 mA cm^{-2})	325.9	91.7% (1000 cycles)	[38]
NiO/Stainless steel mesh	2.5	0.55 (0.75 mA cm^{-2})	211	56% (3000 cycles)	[43]
NiO/graphene MoO_3/Ni foam	0.83	0.85 (10 mA cm^{-2})	708	91.7% (4000 cycles)	[44]
Co_3O_4/N-doped graphene foam	3.0	1.35 (3 mA cm^{-2})	451	95% (1000 cycles)	[45]
MnO_2/Ni foam	18	1.8 (5 mA cm^{-2})	100	90% (1000 cycles)	[46]
$NiCo_2O_4$ @Ni-S/Ni foam	~2.3	1.15 (40 mA cm^{-2})	577	71% (3000 cycles)	[47]
NiO/LSC	~10	10.6 (1 mA cm^{-2}) 4.9 (20 mA cm^{-2})	1064.1 492	80.1% (3000 cycles) (20 mA cm^{-2})	present

3.4. Capacitive performance comparison between NiO/LSC and NiO/Ni-F

To validate the beneficial effect of the 10NiO/LSC, NiO with the same mass loading (10 mg cm^{-2}) loaded on Ni foam (10NiO/Ni-F) is fabricated in a similar way for comparison. The successful preparation of 10NiO/Ni-F is demonstrated with XRD analysis, as shown in Fig. S3a. Figs. 6a and b display the surface SEM images of the 10NiO/LSC and 10NiO/Ni-F, respectively. In contrast to the NiO/LSC in which NiO nanoparticles distribute uniformly on the porous LSC substrate, the NiO on the Ni foam aggregate to form large particles due to the bad wettability of the metal Ni foam

substrate. Similar features can also be observed from their corresponding cross-sectional SEM images, as displayed in Figs. S3b and c.

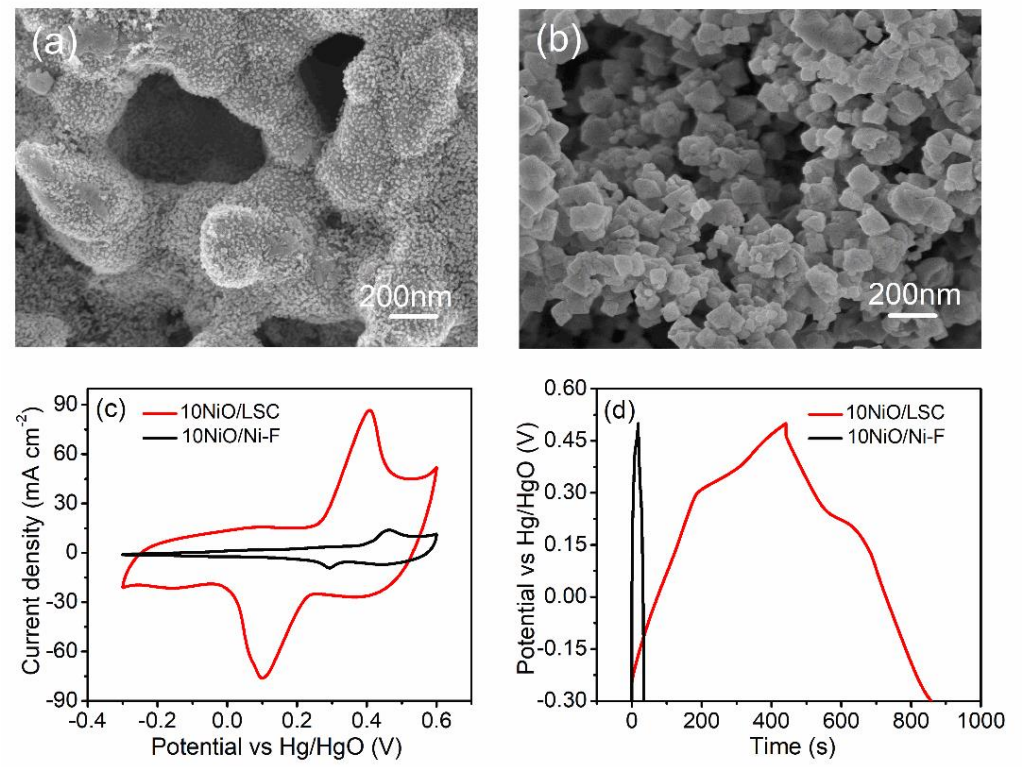

Fig. 6. Surface SEM images of (a) 10NiO/LSC and (b)10NiO/Ni-F. (c) CV curves at a scan rate of 10 mV s^{-1} and (d) galvanostatic charge-discharge profiles at a current density of 10 mA cm^{-2} of 10NiO/LSC and 10NiO/Ni-F.

Fig. 6c shows the CV curves of 10NiO/LSC and 10NiO/Ni-F at a scan rate of 10 mV s^{-1}. Obviously, the enclosed area of the 10NiO/LSC is much larger than that of 10NiO/Ni-F, disclosing higher areal capacitance. A similar conclusion can be obtained from the galvanostatic charge-discharge profiles at a current density of 10 mA cm^{-2}, as shown in Fig. 6d, revealing that 10NiO/LSC possesses a longer discharge time. In consequence, the substrate is essential to the capacitive behaviors of NiO and a porous perovskite-type LSC substrate can provide significantly superior performance than the traditional Ni foam substrate. In fact, though the NiO/LSC electrode is novel and has many advantages, the synthesized ceramic substrate LSC is rigid and fragile compared

to the conventional Ni foam, which may result in its unsuitable for flexible devices. Therefore, it is meaningful to design flexible porous LSC substrate while enable high mass loading of NiO even other active materials in next work.

3.5. Capacitive behavior of asymmetric electrochemical capacitor

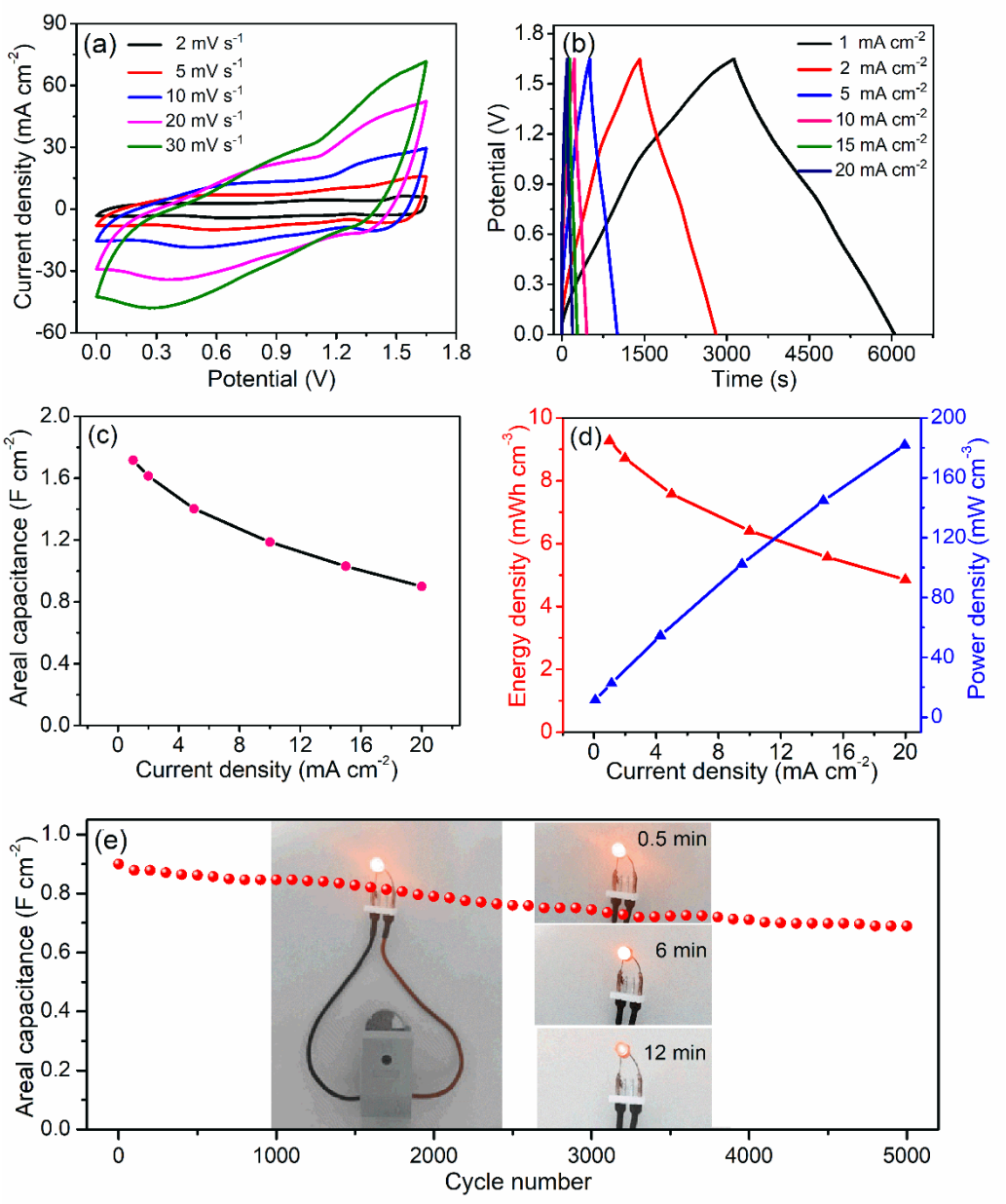

Fig. 7. (a) CV curves, (b) galvanostatic charge-discharge profiles, (c) areal capacitances, (d) Ragone plot at various current densities and (e) cycle performance at 20 mA cm^{-2} (the inset is a photograph that a red LED lighted by two devices in series) of the asymmetric electrochemical capacitor (10NiO/LSC//CC).

To verify the prepared electrode in practical application, an asymmetric electrochemical capacitor is designed with 10NiO/LSC as the positive electrode and CC as the negative electrode, separated by a cellulose paper in an electrolyte solution of 6.0 M KOH. Fig. 7a displays the CV curves at various scan rates under a potential of 1.65 V. The designed device (10NiO/LSC//CC) gives almost quasi-rectangular profiles, implying its capacitive characteristic [48]. Fig. 7b shows the linear and symmetric shape in the charge-discharge process, offering further evidence for the desirable capacitive behavior of the asymmetric electrochemical capacitor. The areal capacitance is calculated based on eq. 1, as presented in Fig. 7c. As observed, the 10NiO/LSC//CC capacitor delivers high areal capacitance of 1.77 F cm^{-2} at 1 mA cm^{-2} and 1.17 F cm^{-2} at 20 mA cm^{-2} (the gravimetric capacitance is displayed in Fig. S4a, respectively, demonstrating a good rate capability (only 33.9% loss)).

Moreover, the volumetric energy density and power density are recorded, as shown in Fig. 7d, to comprehensively estimate the electrochemical performance. The energy density is as high as 9.27 mWh cm^{-3} with a power density of 11.4 mW cm^{-3} at 1 mA cm^{-2}. The power density is up to 181.9 mW cm^{-3} at the high current density of 20 mA cm^{-2}, while the energy density remains 4.86 mWh cm^{-3} (the gravimetric energy density and power density can be seen in Fig. S4b). The energy density of the asymmetric electrochemical capacitor (10NiO/LSC//CC) is much higher than the symmetric or asymmetric devices in previous reports, such as NiO/$Ni(OH)_2$/PEDOT//CMK-3 (1.1 mWh cm^{-3} at 0.4 mA cm^{-2}) [49], Co_9S_8//Co_3O_4@RuO_2 (1.21 mWh cm^{-3} at 2.5 mA cm^{-2}) [50], $NiCo_2O_4$@TiN//$NiCo_2O_4$@TiN (0.083 mWh cm^{-3} at 3 mA cm^{-2}) [51], MnO_2@TiN//activated carbon cloth (1.5 mWh cm^{-3} at 6 mA cm^{-2}) [52] and MnO_2//Fe_2O_3 (0.32 mWh cm^{-3} at 10 mA cm^{-2}) [53].

The cycling durability is also tested under a high current density of 20 mA cm^{-2}. The assembled 10NiO/LSC//CC capacitor retains 76.6% of its origin areal capacitance after 5000 cycles, implying its remarkable stability (Fig. 7e). As shown in the inset of Fig. 7e, two asymmetric devices in series after charging for 1 min at 20 mA cm^{-2} can light a red LED (2.5 V) for ~12 min. The satisfactory electrochemical behaviors of the designed asymmetric capacitor suggest that the NiO/LSC is a promising candidate as a novel electrode for high performance electrochemical capacitors in practical applications.

In fact, the cycling stability of the designed 10NiO/LSC//CC is acceptable, but it is still far from the EDLCs, because the NiO/LSC electrode takes redox reaction during continuous charge-discharge processs, while the EDLCs with excellent cycle stability store energy only through adsorption/desorption of ions at the surface of carbon-based electrode. Another reason for the seemingly relative low durability is caused by the high current density of 20 mA cm^{-2}, which results in inefficient reaction between NiO and NiOOH, leading decrease of the capacitance under long-term electrochemical measurement. Moreover, the cycling stability may be improved by further enhancing the adhesion between NiO nanoparticles and LSC substrate.

4. Conclusions

NiO nanoparticles with a high mass loading (~10 mg cm^{-2}) are directly loaded on a porous perovskite oxide $La_{0.7}Sr_{0.3}Co_{3-\delta}$ ceramic substrate. The binder-free NiO/LSC as a novel electrode for electrochemical capacitors shows excellent capacitive performance, with high areal and specific capacitance (10.6 F cm^{-2} and 1064.1 F g^{-1} at 1 mA cm^{-2}) and remarkable cycling durability (80.1% retention after 3000 cycles at 20

mA cm^{-2}). In addition, the assembled NiO/LSC//CC asymmetric capacitor displays a maximum energy density of 9.27 mW cm^{-3}, preferable rate capability (only 33.9% loss from 1 to 20 mA cm^{-2}) and fine cycling stability (76.6% retention after 5000 cycles at 20 mA cm^{-2}) under a potential of 1.65 V. More realistically, two of the asymmetric devices in series can light a red LED. These attractive findings illustrate that the NiO/LSC electrode can be a competitive alternative for electrochemical capacitors.

Acknowledgments

This work was supported by Guangdong Innovative and Entrepreneurial Research Team Program (No. 2014ZT05N200), National Science Foundation of China (NSFC, No. 21276097), National Science Foundation of China (NSFC, No. U1601207), and Special Funds of Guangdong Province Public Research and Ability Construction (No. 2014A010106008).

References

[1] Wang YG, Song YF, Xia YY. Electrochemical capacitors: mechanism, materials, systems, characterization and applications. Chem Soc Rev 2016;45:5925-5950.

[2] El-Kady MF, Strong V, Dubin S, Kaner RB. Laser scribing of high-performance and flexible graphene-based electrochemical capacitors. Science 2012;335:1326-1330.

[3] Wang GP, Zhang L, Zhang JJ. A review of electrode materials for electrochemical supercapacitors. Chem Soc Rev 2012;41:797-828.

[4] Zhang X, Luo JS, Tang PY, Ye XL, Peng XX, Tang HL, Sun G-S, Fransaer J. A universal strategy for metal oxide anchored and binder-free carbon matrix electrode: a supercapacitor case with superior rate performance and high mass loading. Nano Energy 2017;31:311-321.

[5] Zhai T, Wan L, Sun S, Chen Q, Sun J, Xia QY, Xia H. Phosphate ion functionalized

Co_3O_4 ultrathin nanosheets with greatly improved surface reactivity for high performance pseudocapacitors. Adv Mater 2017;29:1604167.

[6] Zhang Y, Li GY, Lv Y, Wang LZ, Zhang AQ, Song YH, Huang BL. Electrochemical investigation of MnO_2 electrode material for supercapacitors. Int J Hydrogen Energy 2011;36:11760-11766.

[7] Shi ZJ, Xing L, Liu Y, Gao YF, Liu JR. A porous biomass-based sandwich-structured Co_3O_4@Carbon Fiber@Co_3O_4 composite for high-performance supercapacitors. Carbon 2018;129:819-825.

[8] Kumar A, Sanger A, Kumar A, Chandra R. Single-step growth of pyramidally textured NiO nanostructures with improved supercapacitive properties. Int J Hydrogen Energy 2017;42:6080-6087.

[9] Quan HY, Cheng BC, Xiao YH, Lei SJ. One-pot synthesis of α-Fe_2O_3 nanoplates-reduced graphene oxide composites for supercapacitor application. Chem. Eng. J 2016;286:165-173.

[10] Gao LB, Cao K, Zhang HT, Li PF, Song J, Surjadi JU, Li YF, Sun D, Lu Y. Rationally designed nickel oxide ravines@iron cobalt-hydroxides with largely enhanced capacitive performance for asymmetric supercapacitors. J Mater Chem A 2017;5:16944-16952.

[11] Cai GF, Wang X, Cui MQ, Darmawan P, Wang JX, Eh AL, Lee PS. Electrochromo-supercapacitor based on direct growth of NiO nanoparticles. Nano Energy 2015;12:258-267.

[12] Sk MM, Yue CY, Ghosh K, Jena RK. Review on advances in porous nanostructured nickel oxides and their composite electrodes for high-performance supercapacitors. J Power Sources 2016;308:121-140.

[13] Ren B, Fan MQ, Liu Q, Wang J, Song DL, Bai XF. Hollow NiO nanofibers

modified by citric acid and the performances as supercapacitor electrode. Electrochim Acta 2013;92:197-204.

[14] Du HH, Zhou C, Xie XB, Li H, Qi W, Wu Y, Liu T. Pseudocapacitance of nanoporous Ni@NiO nanoparticles on Ni foam substrate: Influence of the annealing temperature. Int J Hydrogen Energy 2017;42:15236-15245.

[15] Cheng S, Yang L, Liu Y, W. Lin, Huang L, Chen DC, Wong CP, Liu ML. Carbon fiber paper supported hybrid nanonet/nanoflower nickel oxide electrodes for high-performance pseudo-capacitors. J Mater Chem A 2013;1:7709-7716.

[16] Singh AK, Sarkar D, Khan GG, Mandal K. Hydrogenated NiO nanoblock architecture for high performance pseudocapacitor. ACS Appl Mater Interfaces 2014;6:4684-4692.

[17] Wu SX, Hui KS, Hui KN, Kim KH. Ultrathin porous NiO nanoflake arrays on nickel foam as an advanced electrode for high performance asymmetric supercapacitors. J Mater Chem A 2016;4:9113-9123.

[18] Yu GH, Xie X., Pand LJ, Bao ZN, Cui Y. Hybrid nanostructured materials for high-performance electrochemical capacitors. Nano Energy 2013;2:213-234.

[19] Gogotsi Y, Simon P. True performance metrics in electrochemical energy storage. Science 2011;334:917-918.

[20] Ricote S, Bonanos N, Lenrick F, Wallenberg R. $LaCoO_3$: Promising cathode material for protonic ceramic fuel cells based on a $BaCe_{0.2}Zr_{0.7}Y_{0.1}O_{3-\delta}$ electrolyte. J Power Sources 2012;218:313-319.

[21] Wu YC, Huang PY, Xu GY. Properties and microstructural analysis of $La_{1-x}Sr_xCoO_{3-\delta}$ (x=0-0.6) cathode materials. Ceram Int 2017;43:2460-2470.

[22] Luo YJ, Wang KC, Zuo JC, Qian QR, Qian YX, Liu XP, Xue H, Chen Q. Selective corrosion of $LaCoO_3$ by NaOH: structural evolution and enhanced activity for

benzene oxidation. Catal Sci Technol 2017;7:496-501.

[23] Brackmann R, Perez CA, Schma M. $LaCoO_3$ perovskite on ceramic monoliths e Pre and post reaction analyzes of the partial oxidation of methane. Int J Hydrogen Energy 2014;39:13991-14007.

[24] Song Y, Sun Q, Lu Y, Liu X, Wang FP. Low-temperature sintering and enhanced thermoelectric properties of $LaCoO_3$ ceramics with B_2O_3-CuO addition. J Alloys Compd 2012;536:150-154.

[25] Li F, Li JF. Effect of Ni substitution on electrical and thermoelectric properties of $LaCoO_3$ ceramics. Ceram Int 2011;37:105-110.

[26] Mineshige A, Inaba M, Yao T, Z. Ogumi. Crystal structure and metal-insulator transition of $La_{1-x}Sr_xCoO_3$. J Solid State Chem 1996;121:423-429.

[27] Mefford JT, Rong X, Abakumov AM, Hardin WG, Dai S, Kolpak AM, Johnston KP, Stevenson KJ. Water electrolysis on $La_{1-x}Sr_xCoO_{3-\delta}$ perovskite electrocatalysts. Nat Commun 2016;7:11053.

[28] Cheng X, Fabbri E, Nachtegaal M, Castelli IE, Kazzi ME, Haumont R, Marzari N, Schmid TJ. Oxygen evolution reaction on $La_{1-x}Sr_xCoO_3$ perovskites: a combined experimental and theoretical study of their structural, electronic, and electrochemical properties. Chem Mater 2015;27:7662-7672.

[29] Petrov AN, Kononchuk OF, Andreev AV, Cherepanov VA, Kofstad P. Crystal structure, electrical and magnetic properties of $La_{1-x}Sr_xCoO_{3-y}$. Solid State Ionics 1995;80:189-199.

[30] Zhang Q, Lu HX, Kawazoe NK, Kawazoe NK. Pore size effect of collagen scaffolds on cartilage regeneration. Acta Biomater 2014;10: 2005-2013.

[31] Cai DP, Wang DD, Wang CX, Liu B, Wang LL, Liu Y, Li QH, Wang TH. Construction of desirable $NiCo_2S_4$ nanotube arrays on nickel foam substrate for

pseudocapacitors with enhanced performance. Electrochim Acta 2015;151:35-41.

[32] Liang J, Tan H, Xiao CH, Zhou GJ, Guo SW, Ding SJ. Hydroxyl-riched halloysite clay nanotubes serving as substrate of NiO nanosheets for high-performance supercapacitor. J Power Sources 2015;285:210-216.

[33] Senthilkumar V, Kadumud FB, Ho NT, Kim JW, Park S, Bae JS, Choi WM, Cho S, Kim YS. NiO nanoarrays of a few atoms thickness on 3D nickel network for enhanced pseudocapacitive electrode applications. J Power Sources 2016;303:363-371.

[34] Zhong JH, Wang AL, Li GR, Wang JW, Ou YN, Tong YX. Co_3O_4/$Ni(OH)_2$ composite mesoporous nanosheet networks as a promising electrode for supercapacitor applications. J Mater Chem 2012;22:5656-5665.

[35] Danilovic N, Subbaraman R, Strmcnik D, Chang KC, Paulikas AP, Stamenkovic VR, Markovic NM. Enhancing the alkaline hydrogen evolution reaction activity through the bifunctionality of $Ni(OH)_2$/metal catalysts. Angew Chem 2012;124:12663-12666.

[36] Kim SI, Lee JS, Ahn HJ, Song HK, Jang JH. Facile route to an efficient NiO supercapacitor with a three dimensional nanonetwork morphology. ACS Appl Mater Interfaces 2013;5:1596-1603.

[37] Tang X, Jia RY, Zhai T, Xia H. Hierarchical Fe_3O_4@Fe_2O_3 core-shell nanorod arrays as high performance anodes for asymmetric supercapacitors. ACS Appl Mater Interfaces 2015;7:27518-27525.

[38] Wang H, Ren Q, Brett DJL, He GJ, Wang RF, Key JL, Ji S. Double-shelled tremella-like NiO@Co_3O_4@MnO_2 as a high performance cathode material for alkaline supercapacitors. J Power Sources 2017;343:76-82.

[39] Simon P, Gogotsi Y, Dunn B. Where do batteries end and supercapacitors begin?

Science 2014;343:1210-1211.

[40] Zhang JF, Wang Y, Shu X, Yu CP, Xiao MF, Cui JW, Qin YQ, Zheng HM, Zhang Y, Chen D, Ajayan PM, Wu YC. One-pot synthesis of nickel-cobalt hydroxyfluorides nanowires with ultrahigh energy density for an asymmetric supercapacitor. Sci Bull 2018;63:322-330.

[41] Kang J, Wen J, Jayaram SH, Yu AP, Wang XH. Development of an equivalent circuit model for electrochemical double layer capacitors (EDLCs) with distinct electrolytes. Electrochim Acta 2014;115:587-598.

[42] Xiang CC, Li M, Zhi MJ, Manivannan A, Wu NQ. A reduced graphene oxide/Co_3O_4 composite for supercapacitor electrode. J. Power Sources 2013;226:65-70.

[43] Shin DH, Lee JS, Jun J, Jang J. Fabrication of amorphous carbon-coated NiO nanofibers for electrochemical capacitor applications. J Mater Chem A 2014;2:3364-3371.

[44] Hou SC, Zhang GH, Zeng W, Zhu J, Gong FL, Li F, Duan HG. Hierarchical core-shell structure of ZnO nanorod@NiO/MoO_2 composite nanosheet arrays for high-performance supercapacitors. ACS Appl Mater Interfaces 2014;6:13564-13570.

[45] Zou YQ, Kinloch IA, Dryfe RAW. Mesoporous vertical Co_3O_4 nanosheet arrays on nitrogen-doped graphene foam with enhanced charge-storage performance. ACS Appl Mater Interfaces 2015;7:22831-22838.

[46] Yang J, Lian LF, Ruan HC, Xie FY, Wei MD. Nanostructured porous MnO_2 on Ni foam substrate with a high mass loading via a CV electrodeposition route for supercapacitor application. Electrochim Acta 2014;136:189-194.

[47] Chu QX, Wang W, Wang XF, Yang B, Liu XY, Chen JH. Hierarchical $NiCo_2O_4$@nickel-sulfide nanoplate arrays for high performance supercapacitors.

J Power Sources 2015;276:19-25.

[48] Feng YY, Zhang HJ, Zhang Y, Bai YJ, Wang Y. Novel peapod NiO nanoparticles encapsulated in carbon fibers for high-efficiency supercapacitors and lithium-ion batteries. J Mater Chem A 2016;4:3267-3277.

[49] Yang HL, Xu HH, Li M, Zhang L, Huang YH, Hu XL. Assembly of $NiO/Ni(OH)_2$/PEDOT nanocomposites on contra wires for fiber-shaped flexible asymmetric supercapacitors. ACS Appl Mater Interfaces 2016;8:1774-1779.

[50] Xu J, Wang QF, Wang XW, Xiang QY, Liang B, Chen D, Shen GZ. Flexible symmetric supercapacitors based upon Co_9S_8 nanorod //Co_3O_4@RuO_2 nanosheet arrays on carbon cloth. ACS Nano 2013;7:5453-5462.

[51] Wang RQ, Xia C, Wei NN. $NiCo_2O_4$@TiN core-shell electrodes through conformal atomic layer deposition for all-solid-state supercapacitors. Electrochim Acta 2016;196:611-621.

[52] Wang W, Liu WY, Zeng YX, Han Y, Yu MH, Lu XH, Tong YX. A novel exfoliation strategy to significantly boost the energy storage capability of commercial carbon cloth. Adv. Mater 2015;27:3572-3578.

[53] Yang PH, Ding Y, Lin ZY, Chen ZW, Li YZ, Qiang PF, Ebrahimi M, Mai WJ, Wong CP, Wang ZL. Low-cost high-performance solid-state symmetric supercapacitors based on MnO_2 nanowires and Fe_2O_3 nanotubes. Nano Lett 2014;14:731-736.